

# A Technique for Detection of PeV Neutrinos Using a Phased Radio Array

A. G. Vieregg<sup>a,b</sup> K. Bechtol<sup>b</sup> A. Romero-Wolf<sup>c</sup>

<sup>a</sup>Department of Physics, Enrico Fermi Institute, University of Chicago,  
5640 S Ellis Avenue, Chicago, IL 60637, USA

<sup>b</sup>Kavli Institute for Cosmological Physics, University of Chicago,  
933 E 56th Street, Chicago, IL 60637, USA

<sup>c</sup>Jet Propulsion Laboratory, California Institute of Technology,  
4800 Oak Grove Drive, Pasadena, CA 91109, USA

E-mail: [avieregg@kicp.uchicago.edu](mailto:avieregg@kicp.uchicago.edu), [bechtol@kicp.uchicago.edu](mailto:bechtol@kicp.uchicago.edu),  
[andrew.romero-wolf@jpl.nasa.gov](mailto:andrew.romero-wolf@jpl.nasa.gov)

**Abstract.** The detection of high energy neutrinos ( $10^{15} - 10^{20}$  eV) is an important step toward understanding the most energetic cosmic accelerators and would enable tests of fundamental physics at energy scales that cannot easily be achieved on Earth. In this energy range, there are two expected populations of neutrinos: the astrophysical flux observed with IceCube at lower energies ( $\sim 1$  PeV) and the predicted cosmogenic flux at higher energies ( $\sim 10^{18}$  eV). Radio detector arrays such as RICE, ANITA, ARA, and ARIANNA exploit the Askaryan effect and the radio transparency of glacial ice, which together enable enormous volumes of ice to be monitored with sparse instrumentation. We describe here the design for a phased radio array that would lower the energy threshold of radio techniques to the PeV scale, allowing measurement of the astrophysical flux observed with IceCube over an extended energy range. Meaningful energy overlap with optical Cherenkov telescopes could be used for energy calibration. The phased radio array design would also provide more efficient coverage of the large effective volume required to discover cosmogenic neutrinos.

---

## Contents

|          |  |           |
|----------|--|-----------|
| <b>1</b> | <b>Introduction</b>  | <b>1</b>  |
| <b>2</b> | <b>A new experimental approach: an in-ice phased radio array</b>                                   | <b>2</b>  |
| 2.1      | Defining a general approach  | 2         |
| 2.2      | Current radio detector techniques  | 3         |
| 2.3      | An in-ice phased array concept   | 3         |
| 2.4      | Example: a 16-channel station  | 5         |
| 2.5      | Achieving An Energy Threshold of 1 PeV   | 8         |
| <b>3</b> | <b>Comparison with current experimental techniques using an independent Monte Carlo simulation</b> | <b>8</b>  |
| <b>4</b> | <b>Conclusions</b>   | <b>11</b> |
| <b>A</b> | <b>Simulation formalism</b>  | <b>12</b> |
| A.1      | Ray-tracing  | 12        |
| A.2      | Sampling neutrino interactions and electric field production                                       | 13        |
| A.3      | Electric field threshold for a fiducial station configuration                                      | 14        |
| <b>B</b> | <b>Simulation diagnostics</b>  | <b>15</b> |

---

## 1 Introduction

The IceCube experiment has recently detected neutrinos of astrophysical origin with energies up to  $\sim 2$  PeV [1]. This is a breakthrough in high energy astrophysics, and represents the first observation of astrophysical neutrinos (except those seen from the sun and supernova 1987a [2, 3]). There are several candidate source classes that could make neutrinos up to 100 PeV, including active galactic nuclei, gamma-ray bursts, and starburst galaxies (for reviews, see [4–6]). In the coming years, we seek to identify the currently unknown sources of PeV astrophysical neutrinos and determine the energy spectrum of those sources to learn about the physics that drives their central engines.

In addition, the detection of ultra-high energy (UHE) neutrinos ( $> 100$  PeV) would open a new window into the universe, allowing us to study distant energetic astrophysical sources that are otherwise inaccessible. UHE neutrinos are created as a byproduct of the so-called GZK process [7], the interaction of a cosmic ray ( $E > 10^{19.5}$  eV) with a cosmic microwave background photon [8, 9]. The current best limit on flux of UHE neutrinos comes from IceCube below  $10^{19.5}$  eV [10], and ANITA above  $10^{19.5}$  eV [11]. Detection of these neutrinos, often called cosmogenic neutrinos, would shed light on the source of the highest energy cosmic rays, tell us about the evolution of high energy sources in our universe, and give us information about the composition of high energy cosmic rays. We expect neutrinos from the GZK process to have extremely high energies, above 100 PeV [12–17]. Detection of UHE neutrinos would also allow us to study weak interactions at center of mass energies  $\gtrsim 100$  TeV, much greater than those available at particle colliders on Earth, such as the

LHC [18–20]. As extremely relativistic particles, UHE neutrinos would enable sensitive tests of Lorentz invariance [21] and other beyond Standard Model processes.

There are clear requirements for an ideal high energy neutrino observatory driven by the twin science goals of determining the origin and spectrum of the observed astrophysical IceCube signal, and discovering cosmogenic neutrinos to determine the origin of the highest energy cosmic rays while also probing particle physics at extremely high energies. The requirements for a high energy neutrino observatory are to 1) have the sensitivity in the PeV energy range to measure the observed IceCube astrophysical neutrino spectrum and extend the measurement to higher energies, 2) have the geometric acceptance at extremely high energies ( $E > 10^{17}$  eV) to detect cosmogenic neutrinos, even in the most pessimistic of reasonable neutrino flux models, 3) have the pointing resolution required (sub-degree) to determine the origin of the observed neutrinos, and 4) have the energy resolution (factor  $\sim 2$ ) required to measure the neutrino energy spectrum at PeV energies and above to learn about the physics that drives the sources of high energy cosmic rays and neutrinos.

One promising way to detect the highest energy neutrinos is through the coherent, impulsive radio emission from electromagnetic showers induced by neutrino interactions in a dielectric — the Askaryan effect [22]. When a neutrino interacts with a dielectric such as ice, an electromagnetic cascade is initiated, and a net negative charge excess develops in the medium. This net charge excess moving faster than the speed of light in the medium yields Cherenkov radiation. For long wavelength, low frequency emission (frequency  $< 1$  GHz), the emission is coherent, and for high energy showers, the radio emission dominates. Beam test measurements [23–25] confirm that the emitted radio power scales as the square of the particle cascade energy and validate the expected angular emission pattern and frequency dependence from detailed numerical simulations [26]. A good medium for detection of high energy neutrinos is a large volume of a dense dielectric with a long radio attenuation length, such as glacial ice, which has an attenuation length  $L_\alpha \sim 1$  km [27, 28].

We introduce here a new type of radio detector for high energy neutrinos that will meet these requirements. In Section 2, we review current radio detector techniques and describe the phased radio array concept. The projected gains in sensitivity using a phased array are presented in Section 3. We conclude in Section 4.

## 2 A new experimental approach: an in-ice phased radio array

### 2.1 Defining a general approach

A high energy neutrino observatory that achieves the goals outlined in Section 1 must have sensitivity over a broad energy range from PeV to  $10^5$  PeV scales. To reach the lowest possible energy threshold, the instrument should be located as close to the neutrino interactions as possible. The electric field strength falls as  $1/r$  (where  $r$  is the distance from the detector to the shower induced by the neutrino interaction) and also suffers attenuation in the detection medium. The lowest threshold will be achieved by a set of detectors that is directly embedded in a detection medium with a long radio attenuation length, such as glacial ice.

To achieve both a low energy threshold and increase the effective volume, the signals used to trigger the detector should have as high an effective gain as possible. High-gain antennas produce a higher signal-to-noise ratio (SNR) per antenna compared to low-gain antennas for radio signals aligned with the boresight, but have reduced angular coverage and may be impractical to deploy down a narrow borehole. Combining signals from multiple low-gain antennas in a phased array provides another way to achieve high gain and therefore

allow weaker neutrino signals to be detected while also allowing full angular coverage. The phased array approach is the topic of this work.

## 2.2 Current radio detector techniques

RICE was a pathfinder experiment for the radio detection of UHE neutrinos and demonstrated the feasibility of many operation-critical technologies [29]. The extremely high energy range, above  $10^{19}$  eV, is currently probed by the ANITA high altitude balloon experiment [30]. The proposed balloon-borne EVA experiment [31] would be a novel way to reach the highest energy neutrinos, above  $10^{19}$  eV. The ARA [32] and ARIANNA [33] experiments, ground-based radio arrays in early stages of development with a small number of stations deployed in Antarctica, have energy thresholds  $\gtrsim 50$  PeV, reaching the heart of the cosmogenic neutrino regime. This is achieved by placing the detectors in the ice.

ANITA, ARA, and ARIANNA all use a similar fundamental experimental design: an array of antennas (16 in the case of ARA) and a data acquisition system comprise a single station. The stations are quasi-independent in that each individual station can reconstruct a neutrino event. ANITA can be viewed as a single-station experiment in this context. For ground-based experiments, multiple stations can be positioned several kilometers apart to cover large volumes of ice, and the neutrino event rate increases linearly with the number of stations.

In current and previously-deployed experiments, a threshold-crossing trigger is used to determine when individual antennas receive an excess in power above typical thermal noise [30, 34, 35]. If a sufficient number of coincident antenna-level triggers occur within a short time window, a station-level trigger is formed, and the antenna waveforms of the candidate neutrino event are digitized and recorded. Essentially this type of combinatoric threshold-crossing trigger is only sensitive to the amount of power seen by individual antennas as a function of time. With this triggering approach, the smallest signal that a station can see is determined by the gain of each individual antenna (i.e., how much power the antenna sees from signal compared to thermal noise).

## 2.3 An in-ice phased array concept

We present here a new concept for radio detection of high energy neutrinos that will for the first time have sensitivity in the 1 PeV energy range, allowing us to characterize the measured IceCube astrophysical neutrino spectrum, extend the measurement to higher energies, and achieve meaningful overlap with IceCube in energy for energy calibration. This new radio detector would also achieve improved sensitivity in the UHE regime per station, provide superior pointing resolution at all energies, and provide stronger rejection against anthropogenic radio frequency interference compared to currently-implemented radio techniques.

The key to lowering the energy threshold of a radio experiment and increasing sensitivity at higher energies is the ability to distinguish weak neutrino-induced impulsive signals from thermal noise. For antennas triggering independently, the amplitude of the thermal noise is solely determined by the temperature of the ice and the noise temperature of the amplifiers (a smaller effect than the ice itself).

Combining signals from many antennas in a phased array configuration averages down the uncorrelated thermal noise from each antenna while maintaining the same signal strength for real plane-wave signals (such as neutrinos). If we combine the signals from multiple antennas with the proper time delays to account for the distance between antennas, we can effectively increase the gain of the system of antennas for incoming plane waves from a

given direction. Many different sets of delays with the same antennas can create multiple effective antenna beam patterns that would together cover the same solid angle as each individual antenna but with much higher gain. This procedure is called beamforming, and is an economical and efficient way to achieve the extremely high effective gain needed to push the energy threshold down to 1 PeV. Such interferometric techniques have been extensively used in radio astronomy (for a review, see [36]).

The effective gain  $G_{\text{eff}}$  in dBi or dBd of the system is determined by the gain of each individual antenna in dBi or dBd,  $G$ , and the number of antennas,  $N$ , by:

$$G_{\text{eff}} = 10 \log_{10}(N \times 10^{G/10}). \quad (2.1)$$

The trigger threshold of radio detectors is typically set by the rate at which antenna waveforms can be digitized and recorded while maintaining a high livetime fraction. Lower thresholds on the electric field at the antennas correspond to both increased efficiency for neutrino signals and higher trigger rates. For a phased array, each trigger channel corresponds to a single effective beam, and the station-level trigger is the union of simple threshold-crossing triggers on the individual effective beams of the phased array, rather than individual antennas. In this configuration, the threshold on the electric field could be reduced by roughly the square root of the number of antennas that are phased together while maintaining the same overall trigger rate per trigger channel. Since the electric field produced at the antenna from Askaryan emission scales linearly with the energy in the particle cascade, this reduction in the effective electric field threshold directly translates into a lower energy threshold for finding neutrinos. Equivalently, the effective volume of the detector is increased at fixed neutrino energy since events could be detected from farther away. To minimize the number of trigger channels, thus minimizing complexity and cost, the phased array that provides the trigger needs to be as closely packed as possible. Since the overall physical size of the array compared to the wavelength of radiation determines the angular resolution of the instrument, the closer the spacing between antennas, the larger each effective beam is for a given frequency of radiation, and the fewer channels are required to cover the same solid angle of ice [36].

Further sensitivity gains may be possible by recognizing that the antennas that form the trigger do not have to be the same antennas used for detailed event analysis. Indeed, it is advantageous to construct two distinct, co-located antenna arrays. The first is the phased array that is as closely packed as possible and provides the most sensitive trigger possible (the “trigger array”). The second array is a set of antennas that are spaced as far apart as is reasonably possible (many tens of meters) to provide the best pointing resolution and energy resolution possible for neutrino events (the “pointing array”). Although the station triggers on the compact trigger array, we do not need to digitize and record signals from those antennas – instead, we digitize and record signals from the much farther spaced pointing array based on the timing given by the trigger. The compact trigger array also has the benefit that the position of the antennas only needs to be determined to within a few inches in order to phase the antennas properly. The distinct sets of antennas that comprise the pointing array and the trigger array enable both optimal sensitivity and optimal directional pointing and energy reconstruction compared to the scenario where one compromises both technical goals in order to find middle ground that uses the same antennas for the trigger and pointing. This two-component station design represents a departure from all previous radio detector neutrino experiments.

The phased trigger array also has the benefit that it can help reject anthropogenic radio frequency interference. A low-gain antenna has a very wide beam pattern, and is sensitive to

many incoming directions of radiation. However, a high-gain antenna, such as is effectively created by the phased trigger array, is highly directional. Since this configuration would have many effective high-gain beams, each pointed in a different direction, at any given time we can easily mask out directions where there is man-made interference from the trigger. Since man-made noise tends to come from specific incident directions corresponding to the location of sources of noise, the ability to mask out directions from the trigger improves background rejection and allows the threshold of the trigger to be set by thermal noise for a larger fraction of time, rather than the threshold increasing when more man-made radio frequency interference is present.

Equation 2.1 holds for the case where the signal is amplified with a low-noise amplifier for each antenna before the beams are formed (i.e., the noise contribution from each channel is the same and no significant noise is introduced after the beams are formed). If the loss in the system is low enough, the first stage of amplification could be performed after the beams have been formed, so each beam has a noise contribution from only one amplifier. This improvement would come at the cost of including any noise from loss in the cables and the beamforming components. In a typical case, the array views 250 K ice and the front-end system has a temperature of 70 K. Even if the beamforming hardware were lossless, the improvement in overall system temperature is small, approaching 10% improvement only after phasing 400 antennas, since the noise from the ice dominates the noise from the amplifier system. Despite only modest potential improvements, this technique may ultimately allow for fewer front-end amplifiers to be used, which would reduce the cost of the array.

An interferometric technique has been previously developed and used in post-processing analysis for fast, impulsive radio signals from neutrino interactions. This interferometric technique was first developed for and applied to the ANITA experiment [37], and has since been applied to other experiments [34, 38]. Interferometric techniques have also been used to search for extremely high energy neutrinos, above  $10^{22}$  eV, using the Westerbork Radio Synthesis Telescope and the moon as a target [39].

There have been efforts directed toward reconfiguring the triggering scheme of currently-deployed or soon-to-be deployed experiments, such as ANITA and ARA, to instead use real-time correlation triggering after 3-bit digitization of the Nyquist-sampled waveforms [40]. This technique is under development, and is expected to be used in the upcoming fourth flight of ANITA. There are two reasons why one should consider doing the beamforming in hardware. The first is that it leaves open the possibility of doing the signal amplification after the beams are formed to reduce the noise contribution from the front-end electronics. The second is that information is lost in the 3-bit digitization that is preserved by doing the full phasing in hardware.

As described above, the optimization of the geometry of a station should be different for a phased radio array compared to currently-deployed instruments to fully exploit the power of the beamforming technique. We explore here two scenarios: the first is a 16-channel station much like the deployed stations for the ARA experiment but with a different geometry and with the phased array trigger implemented, and the second is a 400-channel station that would achieve a 1 PeV threshold.

## 2.4 Example: a 16-channel station

We introduce here the example of a 16-channel station that uses dipole-like antennas and is deployed down boreholes beneath the firn layer of a deep glacier. Possible sites for such a station, or set of stations, include South Pole, where the array would be  $\sim 200$  m below the

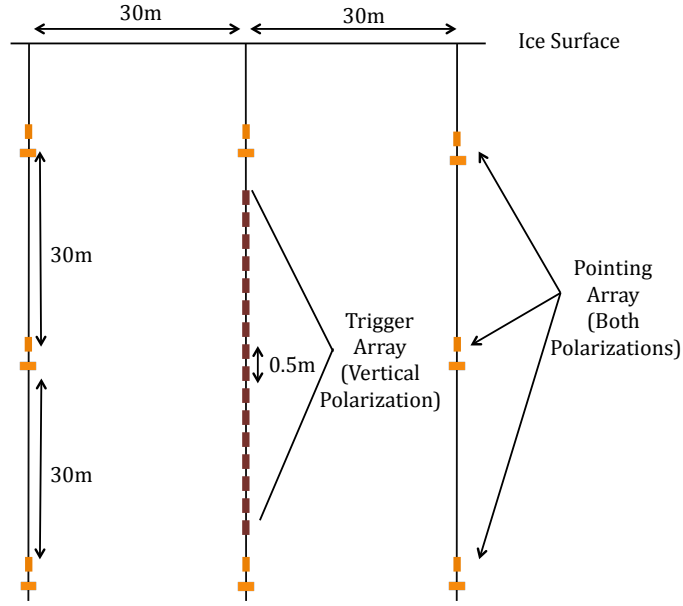


**Figure 1.** An example station layout for a 16-antenna phased trigger array and accompanying pointing array.

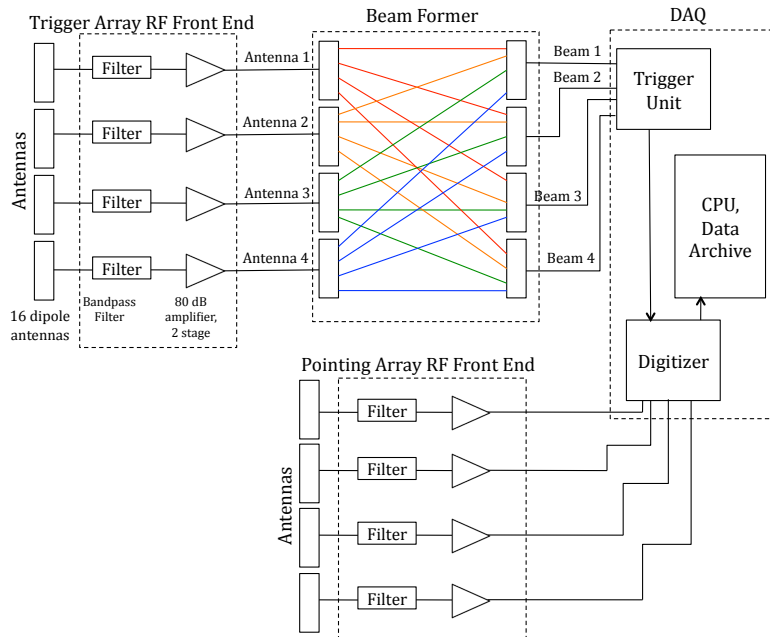


**Figure 2.** An example layout of the radio frequency chain of a 16-antenna phased trigger array and accompanying pointing array. For simplicity, not all channel paths are depicted.

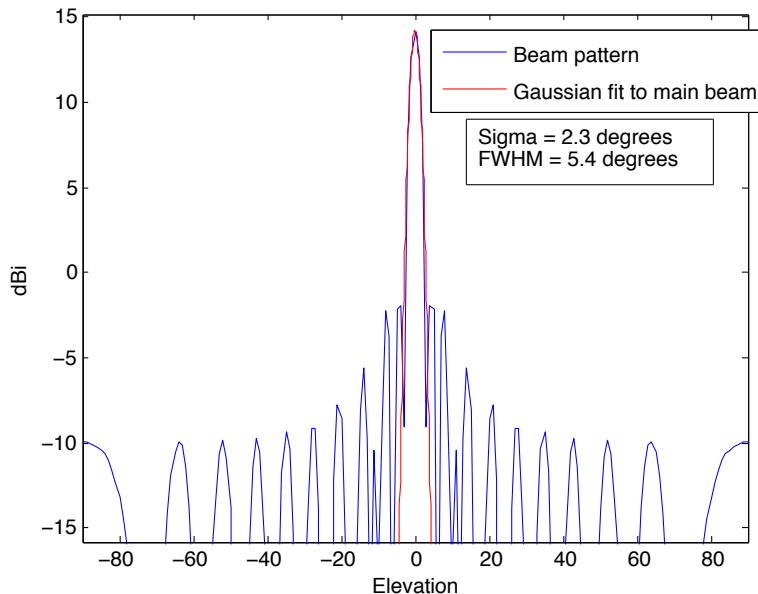


**Figure 3.** The beam pattern for one trigger channel at 200 MHz for the configuration shown in Figure 1.

surface and the ice is  $\sim 2.8$  km deep [41, 42], and Summit Station in Greenland, where the array would be  $\sim 100$  m below the surface and the ice is  $\sim 3.0$  km deep [43].

We simulate a configuration where the antennas are deployed down boreholes below the firn. Our simulations confirm the finding from ARA [32, 34] that due to the changing index of refraction in the firn as the glacial ice transitions to snow, incident radio emission is often deflected downwards away from a detector on the surface and is therefore undetected (see A.1 for details). In contrast, receivers deployed below the firn layer are less affected by refraction and the increase in effective volume compared to a surface configuration is large (factors of 3 to 10 depending on the firn profile). The benefits of borehole-deployed antennas make them a cost effective approach.

One possible station layout is shown in Figure 1. A trigger array is constructed of 16 dipole antennas strung vertically down one borehole as close together as possible. This configuration would naturally be sensitive to vertically-polarized signals, although one could combine signals from orthogonally-polarized antennas to create an unpolarized trigger. The pointing array would be constructed of additional antennas, with both horizontal and vertical polarization sensitivity, and would require at least two additional boreholes to uniquely determine the incident direction, timing, and polarization of the radio emission and thus the incoming direction of the neutrino. We would only need to digitize the signals from the pointing array antennas. An example of the radio frequency chain for a 16-antenna station is shown in Figure 2.

The effective gain of such a 16-channel trigger array of dipole antennas calculated using Equation 2.1 is 14.2 dBi (compared to 2.15 dBi for a single dipole), which corresponds to a factor of  $\sim 4$  in electric field threshold. The effective beam at 200 MHz for one trigger channel is shown in Figure 3 as a function of elevation. The FWHM of the beam of a single trigger channel is  $5.4^\circ$  in elevation with complete azimuthal coverage for this configuration. By



adjusting the delays among antennas in different trigger channels, we can cover the relevant range of solid angle for incoming emission from visible neutrino events with only  $\sim 15$  beams. Antennas with a moderately higher gain that still cover the relevant range of solid angles would lead to a higher effective gain of the system.

## 2.5 Achieving An Energy Threshold of 1 PeV

The phased array design is scalable and can be configured to achieve an even lower energy threshold. For example, a phased array with 400 dipole antennas would have an effective gain of 28.2 dBi, and would push the electric field threshold down by a factor of  $\sim 20$  compared to currently-implemented techniques. For large numbers of antennas, the single-borehole configuration for the trigger array is no longer optimal. To keep the size of the trigger array compact, trigger antennas would be deployed down multiple boreholes. Phased arrays with thousands of channels are possible.

Since the spectrum and angular distribution of Askaryan emission is largely independent of the neutrino energy [44], the same experimental design principles and simulation methods are valid over the large range of neutrino energies we consider.

## 3 Comparison with current experimental techniques using an independent Monte Carlo simulation

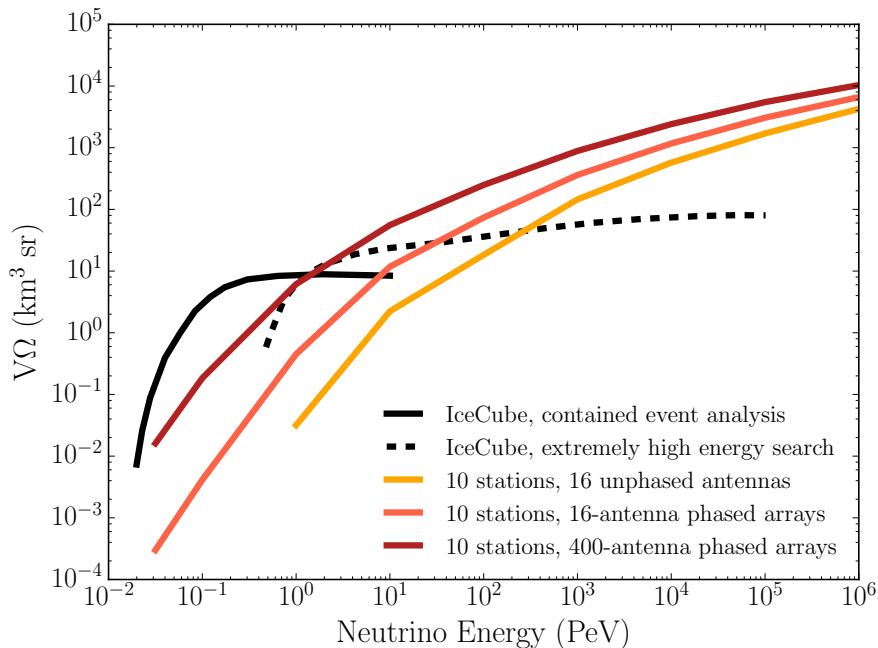


**Figure 4.** Effective Volume vs. Energy for 10 stations installed 100 m below the surface at Summit Station, Greenland. The yellow line is for 16-channel stations with no phasing, the orange line is for similar stations but with phasing, and the red line is for 400-antenna phased array stations. For each radio array configuration, the volumetric acceptance is presented at the trigger level. Black curves indicate the volumetric acceptance for two difference analyses with IceCube optimized for different energy ranges [45, 46].

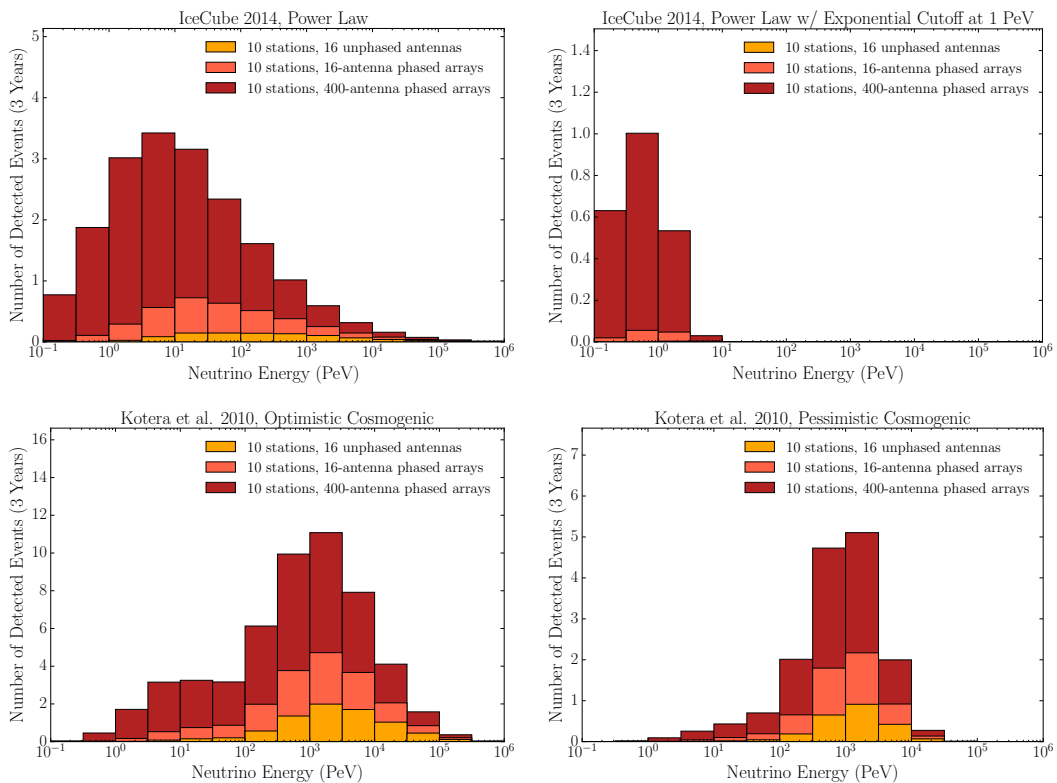


**Figure 5.** Triggered Event Rates vs. Energy for a variety of neutrino models. Triggered event rates for three years of observation for 10 stations installed 100 m below the surface at Summit Station, Greenland. 16-channel stations with no phasing are shown in yellow, 16-channel stations with phasing are shown in orange, and stations with 400 phased antennas are shown in red. The top two panels show event rates based on two possible neutrino spectra based on the IceCube observed neutrino flux [1]. The top left panel is an  $E^{-2.3}$  power law, and the top right panel is an  $E^{-2.3}$  power law with an exponential cutoff at 1 PeV. The bottom two panels show event rates based on optimistic and pessimistic cosmogenic fluxes [17].

We have developed a Monte Carlo simulation package to quantify the acceptance of various radio detector configurations, and more specifically, investigate the advantages of a phased array design. The simulation formalism and assumed physics input are described in A, and validation studies are presented in B. Rather than focusing on specific antenna designs, signal processing chains, and analysis algorithms, we have kept the simulations general by defining signal detection thresholds in terms of the electric field strength arriving at the antennas. In this case, different station configurations correspond to different electric field thresholds, as described above. The parameters chosen to define the electric field threshold of our baseline station configuration are discussed in A.3. Depending on the particular system deployed, the overall results could shift up or down (by less than a factor of two), but the relative comparisons between configurations are valid.

Figure 4 shows the volumetric acceptance of a 10 station detector with antennas 100 m below the surface at Summit Station as a function of energy for three different configurations: 16-channel stations with no phasing (yellow), 16-channel stations with phasing (orange), and 400-antenna phased array stations (red). See A for a description of how effective volume

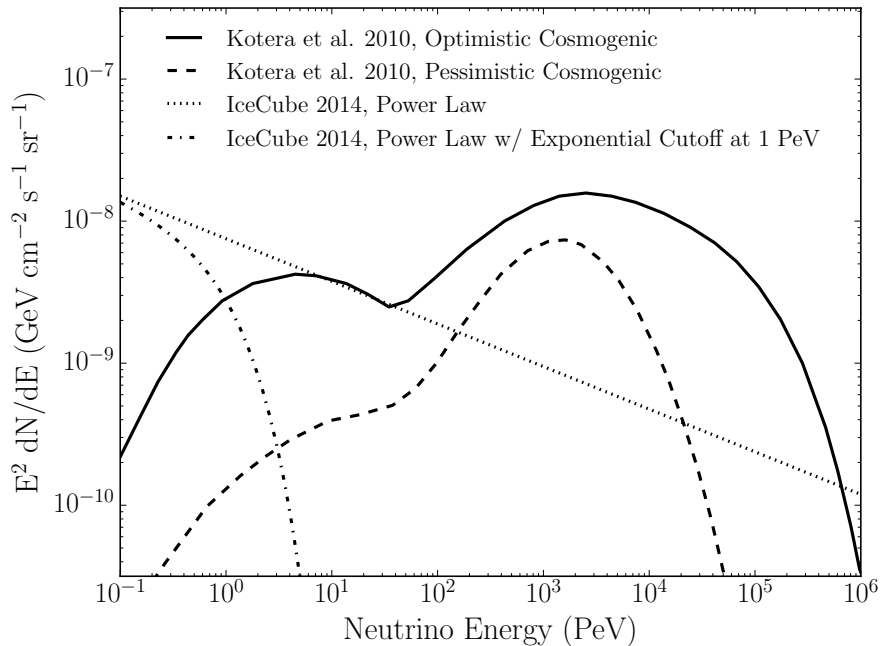


**Figure 6.** Flux models used for the predictions shown in Figure 5. Shown are two possible neutrino spectra based on the IceCube observed neutrino flux [1]: an  $E^{-2.3}$  power law and an  $E^{-2.3}$  power law with an exponential cutoff at 1 PeV. Also shown are optimistic and pessimistic cosmogenic fluxes [17].

is calculated. We also show for comparison the acceptance corresponding to two IceCube analyses optimized for different energy ranges, calculated using the effective area given in [45, 46] and the neutrino interaction cross section given in A. The IceCube curves in the figure include analysis efficiency, whereas the results of our simulation do not, so the curves are not directly comparable. The standard method, shown with the yellow line in Figure 4, is comparable to the approach of the ARA experiment but with only 10 stations [32].

For this study, we have chosen to simulate the experiment at Summit Station in Greenland. Moving the detectors to South Pole at a depth of 200 m below the surface would increase the acceptance by  $< 20\%$  due to a longer radio attenuation length in ice at the South Pole [27]. We have chosen to simulate 10 stations for this study, but we note that the acceptance changes linearly with the number of stations, since stations trigger independently.

Figure 5 shows the number of events detected as a function of energy for the same three detector configurations shown in Figure 4 for a variety of astrophysical and cosmogenic models. We show event rates for an  $E^{-2.3}$  power law based on IceCube observations [1], an  $E^{-2.3}$  power law with a 1 PeV exponential cutoff [1], and optimistic and pessimistic cosmogenic models [17]. The flux models used for Figure 5 are shown in Figure 6. Table 1 summarizes the expectation values for the total number of events detected with each detector configuration for each model. A harder spectrum for PeV-scale neutrinos would yield a higher event rate.

For the most pessimistic cosmogenic neutrino flux models (not shown in Figures 5, 6, or Table 1) with no source evolution and a pure iron composition for UHE cosmic rays [17], the expected event rate with 10 stations of 400 phased antennas each is  $\sim 0.1$  event per year. However, recent measurements with Pierre Auger Observatory and the Telescope Array

| Station Configuration | Power Law | Power Law with Cutoff | Optimistic Cosmogenic | Pessimistic Cosmogenic |
|-----------------------|-----------|-----------------------|-----------------------|------------------------|
| 16-antenna            | 0.9       | 0.0                   | 7.7                   | 2.3                    |
| 16-antenna, phased    | 3.8       | 0.1                   | 19.6                  | 6.0                    |
| 400-antenna, phased   | 18.4      | 2.2                   | 52.9                  | 15.6                   |

**Table 1.** Expectation values for the total number of triggered events in 3 years for 10 stations in different configurations for spectra based on IceCube observations [1] and for cosmogenic models [17].

disfavor a significant iron fraction in the cosmic ray composition at energies up to and even exceeding  $10^{19.5}$  eV [47, 48], so we do not discuss these cosmogenic models further in this work.

By phasing the antennas in a 16-antenna array, we have improved the UHE neutrino event rate by more than a factor of two over the non-phased case, and extended the sensitivity to lower energies. The 16-antenna phased configuration achieves a low enough energy threshold to distinguish an  $E^{-2.3}$  power law extrapolation of the observed IceCube spectrum from one that has a cutoff at the PeV scale. Phasing more antennas lowers the threshold even further, and makes marked improvements in event rates, especially at low energies (see the 400-antenna configuration in Table 1 and Figure 5). Increasing the number of stations results in a linear increase in the expected number of events.

As is evident in Figure 4, 10 stations of 16-antenna phased arrays have a larger acceptance than IceCube above 30 PeV, and the acceptance grows faster with energy than IceCube, so that by  $10^{18}$  eV the acceptance is an order of magnitude more than IceCube. 10 stations of the 400-antenna phased arrays have a larger acceptance than IceCube above 1 PeV.

## 4 Conclusions

We have described a new concept for an in-ice phased radio array that is designed to achieve sensitivity to the astrophysical neutrino flux at 1 PeV and above, provide energy overlap with IceCube for calibration, and discover cosmogenic neutrinos in an efficient way. It is worth noting the scalability of the radio technique for increasing acceptance at all energies. The acceptance increases linearly with the number of stations, and further gains can be realized by phasing more antennas in each station, particularly at PeV neutrino energies. An array of 100 stations each with 400-antenna phased arrays could detect hundreds of neutrinos at PeV energies and above each year. Such an experiment would revolutionize our view of the high-energy universe.

## Acknowledgments

This work was supported by the Kavli Institute for Cosmological Physics at the University of Chicago. Computing resources were provided by the University of Chicago Research Computing Center. Part of this research was carried out at the Jet Propulsion Laboratory, California Institute of Technology, under a contract with the National Aeronautics and Space Administration. We would like to thank A. Connolly, P. Gorham, D. Saltzberg, and S. Wissel for useful conversations and guidance.

## A Simulation formalism

We used numerical Monte Carlo simulations to evaluate the acceptance of different array configurations considered in this work. The individual stations of the array were assumed to be widely spaced such that a given neutrino interaction is unlikely to be detected with multiple stations. In this limit, the stations act independently and it is possible to simulate the response of a single station and multiply the derived acceptance by the total number of stations in the array to obtain the total acceptance (see, e.g., [32]). We also assumed that the ice properties depend only on depth such that a cylindrical coordinate system with azimuthal symmetry can be defined. To provide a concrete example, we used Summit Station, Greenland as the site of the envisioned radio array and considered stations at a depth of 100 m, i.e., just below the firn layer [43].

### A.1 Ray-tracing

The simulations were performed in two stages for computational efficiency. First, we generated a library of ray-tracing solutions for radio waves propagating through the ice sheet. Rays originating at the particle cascade must intersect the station in order to be detected. This boundary condition implies that a complete set of viable ray-tracing solutions can be found by following rays launched at varying zenith angles from the station in the time-reverse sense. The trajectories are curved due to the varying index of refraction in different layers of the ice, and reflections can occur both at the ice-air interface at the top of the glacier and the ice-rock interface at the base of the glacier. Measurements of the firn density profile (upper 100 m) at Summit Station show that the index of refraction at  $\sim 300$  MHz is correlated to the vertical density profile determined from ice cores through the relation  $n = 1 + k\rho$  with  $k = 8.45 \times 10^{-4} \text{ kg}^{-1} \text{ m}^3$  [49]. We applied the same formula to density profiles from GISP2 ice core data [43] to estimate the index of refraction throughout the ice sheet. Figure 7 shows ray-tracing solutions for a station located at a depth of 100 m. The density profile changes rapidly in the firn layer of the ice sheet and therefore ray bending is expected to be most pronounced in the upper  $\sim 100$  m of the ice sheet. This effect results in a “firn shadow” region that is inaccessible except through reflections at the bottom of the ice sheet [50].

At short propagation distances from the station, there are three distinct sets of continuous solutions that define regions in which different classes of ray-tracing solutions exist. The first class involves reflections off the ice-air interface. The latter two classes involve rays that do not reach the surface, but which can cross over each other due to different amounts of refraction in the firn. It is useful to distinguish between these two classes to recognize regions where two viable ray-tracing solutions corresponding to different zenith angles exist. The three solution classes are doubled when also considering rays that reflect off the bottom of the ice sheet, resulting in a total of six solution classes.

At each step along a given ray-tracing solution, which are spaced from 1 ns to 5 ns in time depending on the differential index of refraction, we record the location, propagation distance, direction of propagation, and the cumulative attenuation to the station separately in horizontal and vertical polarization. We used the radio attenuation length measurements at Summit Station from [27]. Fresnel conditions are applied to compute the reflected power at the ice-air and ice-rock interfaces.

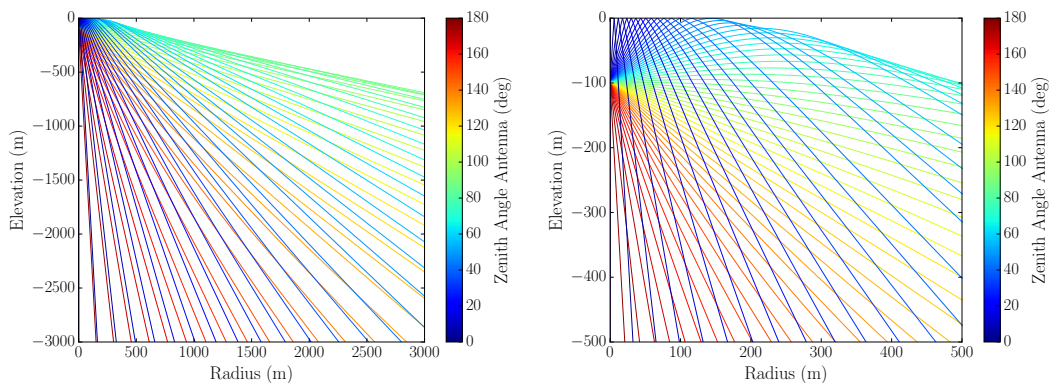


**Figure 7.** A ray-tracing diagram for antennas 100 m below the surface of the ice at Summit Station in Greenland. The left shows the full depth of the glacier (3000 m), and right is a detailed view close to the station. For a given zenith angle of the ray at the antenna, there are three solutions for the true incident radiation direction as discussed in the text. Including waves that reflect off of the ice-rock interface at the bottom of the glacier doubles the number of solutions. The second set of solutions are not shown here. The color indicates the zenith angle at which the antenna sees the ray.

## A.2 Sampling neutrino interactions and electric field production

In the second stage of the simulations, we randomly generated neutrino interaction geometries within a cylindrical target volume centered on the station and used the ray-tracing library described above to compute the electric field that would be produced at the antennas. Neutrino interaction vertices were selected uniformly throughout the target volume and arrival directions were uniformly distributed over the celestial sphere ( $4\pi$  sr). For computational efficiency, the size of the target volume,  $V_{\text{sim}}$ , was enlarged for the highest neutrino energies and contracted for lower neutrino energies. In all cases, the depth was matched to the thickness of the ice sheet (3000 m) and the radius was chosen to be large enough to encompass all detectable events.

We focused on neutrino-induced hadronic cascades when computing the Askaryan emission. Muons and tau leptons produced in charged-current interactions are expected to deposit their energy in elongated tracks that would be difficult to detect [51], and the electromagnetic cascade from charged-current interactions of UHE electron neutrinos can be elongated due to the Landau-Pomeranchuk-Migdal (LPM) effect [26, 52, 53], resulting in a narrow Cherenkov emission cone [54]. Hadronic cascades are less affected by elongation due to the LPM effect, and the width of the Cherenkov cone is therefore less dependent on neutrino energy [44, 55]. In addition, simulations of the LPM effect at higher energies have been shown to produce cascades with interfering pulse trains rather than elongated pulses [56]. With the high gain provided by an in-ice phased array, these signals could be more readily differentiated from the thermal noise background. Estimating the increase in acceptance due to these signals will be the subject of a future study. Either way, the approach taken here is conservative since the LPM effect will only become dominant for electromagnetic showers with energies  $> 10^{18}$  eV.

For each candidate neutrino event, we determined viable ray-tracing solutions by interpolating between rays within each respective class of solutions in the ray-tracing library (see above). Next, for each viable ray-tracing solution, we used the analytic parametrization of [57] to compute the Askaryan emission at the unique angle between the neutrino propaga-

tion direction (parallel to the cascade development) and the ray connecting the cascade to the station. We used a characteristic length scale for the shower of 1.5 m, as suggested by [57]. When computing the fraction of the incident neutrino energy that is visible in the cascade, we used the analytic parametrizations for the inelasticity (Bjorken- $y$  parameter) from [19], which corresponds to the energy in the hadronic cascade. The inelasticity distributions for neutral current and charged current interactions of both neutrinos and anti-neutrinos are expected to be nearly indistinguishable in the UHE range. For simplicity, we drew values from the inelasticity distribution for charged-current neutrino interactions.

In the UHE regime, the neutrino-nucleon interaction cross section is sufficiently large that a significant fraction of upward-going neutrinos interact while passing through the solid body of the Earth and are therefore not detectable. We used the analytic parametrizations for the interaction cross section from [19] and the Preliminary Reference Earth Model (PREM) profile for the Earth’s density [58] to compute the probability  $p_{\text{Earth}}$  that neutrinos survive passage through the Earth as a function of their energy and incoming zenith angle. The Earth passage probability takes into account the distance traversed through the ice sheet on the way to interaction vertex. For the purpose of computing the neutrino interaction probability, we used the total interaction cross section for neutrinos (as opposed to anti-neutrinos). In the energy range considered here, the total cross section for neutrinos is a factor of 1.06 to 1.25 larger than for anti-neutrinos. The current simulations do not include the cross section enhancement from the Glashow resonance,  $\bar{\nu}_e e \rightarrow W^-$ , which would lead to a further enhancement in acceptance for electron anti-neutrinos of energy  $\sim 6.3$  PeV [59–61].

The process described above effectively samples the instrumental sensitivity over the detector volume and all possible arrival neutrino directions. A minimum of  $10^6$  candidate neutrino events were processed in each of 17 logarithmic steps ranging from  $10^{13}$  eV to  $10^{21}$  eV separated by 0.5 decades in neutrino energy. The all-sky water-equivalent volumetric acceptance ( $\text{km}^3 \text{sr}^{-1}$ ) was then calculated for each energy as

$$V\Omega = \frac{4\pi V_{\text{sim}}}{N} \times \sum_i \left( p_{\text{Earth},i} \times p_{\text{detect},i} \times \frac{\rho_i}{\rho_{\text{water}}} \right), \quad (\text{A.1})$$

with  $i$  iterating over neutrino events.  $p_{\text{detect},i}$  denotes probability that the electric field at station results in a trigger (see A.3).  $\rho_i$  is the ice density at the interaction vertex and  $\rho_{\text{water}}$  is the density of water. To compute the event rate for various neutrino flux models, the sensitivity can be equivalently expressed in terms the areal acceptance ( $\text{m}^2 \text{sr}^{-1}$ ) as

$$A\Omega = V\Omega/l, \quad (\text{A.2})$$

where  $l$  is the neutrino interaction length through water using the total interaction cross section [62].

### A.3 Electric field threshold for a fiducial station configuration

The final step of evaluating the neutrino acceptance is to determine which events pass the trigger. For generality, we used a simple threshold on the electric field produced at the antennas to define a trigger criterion and we compare the acceptance of various station configurations at the trigger level. For each case that we simulated, we assume the same fixed trigger rate per channel.

We assume a bandwidth of 100–800 MHz and compute the signal electric field strength by integrating the Askaryan emission over this frequency range. As explained in detail below,

an electric field trigger threshold of 0.15 mV/m per antenna is equivalent to a  $2.3\sigma$  trigger threshold for ideal dipole antennas with the assumed bandwidth.

The root mean square voltage received in a system ( $V_{\text{RMS}}$ ) for thermal noise is

$$V_{\text{RMS}} = \sqrt{k_{\text{B}}TBZ}, \quad (\text{A.3})$$

where  $T$  is the total system temperature,  $B$  is the bandwidth of the system,  $Z$  is the impedance of the system, and  $k_{\text{B}}$  is Boltzmann's constant. Assuming a system temperature of 70 K in addition to the temperature of the ice (250 K), a bandwidth of 700 MHz, and a  $50\Omega$  system impedance, we calculate that  $V_{\text{RMS}} = 12.6\mu\text{V}$ . This thermal noise contribution sets the threshold of the system.

The electric field threshold is given by

$$E = V\sqrt{\frac{Z_0}{A_{\text{eff}}Z}}, \quad (\text{A.4})$$

where  $V$  is the voltage received,  $A_{\text{eff}}$  is the effective area of the antenna, and  $Z_0$  is the impedance of free space [63, 64].  $A_{\text{eff}}$  is defined as

$$A_{\text{eff}} = \frac{\lambda^2 G}{4\pi}, \quad (\text{A.5})$$

where  $G$  is the antenna gain, and  $\lambda$  is the wavelength. For a  $50\Omega$  system, the electric field threshold is therefore given by

$$E = V\frac{9.73}{\lambda\sqrt{G}}. \quad (\text{A.6})$$

Assuming a perfect dipole antenna with a gain of 2.15 dBi and a fast impulse response, a reference frequency of 200 MHz, and a trigger threshold of  $2.3\sigma$  above thermal noise, we calculate an electric field threshold per trigger channel of 0.15 mV/m, which is the same as the per-antenna threshold for the 16-antenna station configuration without phasing.

The final acceptance for a detector must also include the efficiency of successfully reconstructing events and discriminating signal from thermal noise and anthropogenic backgrounds. Previous radio detection experiments have achieved high analysis efficiencies relative to the trigger-level efficiency, e.g., a 96% reconstruction efficiency for ANITA [11]. Despite a lower signal-to-noise per antenna expected in a phased array configuration, the opportunity to position in-situ stations in stable, low-noise environments as well as directional rejection of backgrounds (Section 2.3) could result in comparably high analysis efficiencies.

## B Simulation diagnostics

As a basic validation of the simulation output and to develop an intuition for the instrument response, we compare the distributions of several triggered event properties for different station configurations. We investigate here two different energies (1 PeV and 1000 PeV) and the three different experimental configurations we have discussed in this paper (16-channels not phased, a 16-antenna phased array, and a 400-antenna phased array).

Figure 8 shows the distribution of the distance from the antennas to the interaction vertex as measured along the radio signal path for each event that satisfies the trigger requirements. As expected, lower energy events occur closer to the detector and station configurations with lower thresholds are capable of triggering on more distant events.



The angle at which the detector views events relative to their neutrino propagation direction is shown in Figure 9. The Cherenkov angle is shown for reference as a dashed line. As expected, higher energy events are seen farther from the Cherenkov angle. Configurations with lower threshold (e.g., phased arrays) also allow for events to be seen farther from the Cherenkov angle where the emission is weaker.

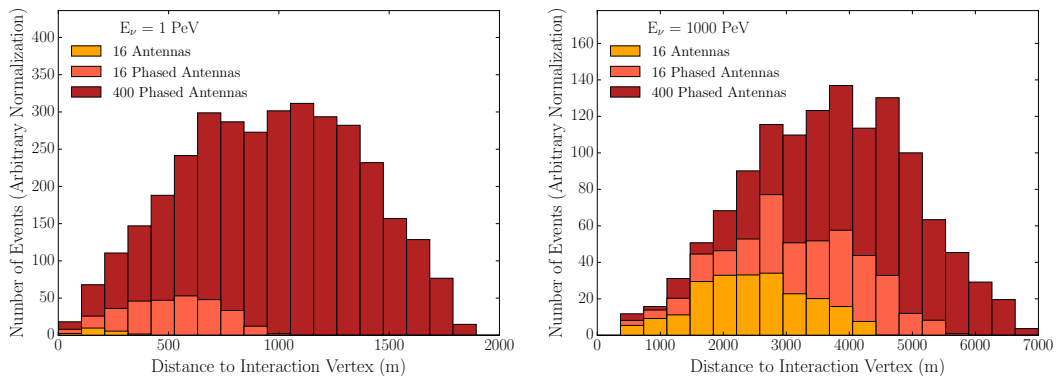


**Figure 8.** The distance from the antennas to the interaction vertex for passing events at two different energies (1 PeV and 1000 PeV) and the three different experimental configurations we have discussed (16-channels not phased, a 16-antenna phased array, and a 400-antenna phased array). Lower energy events occur closer to the detector, and a phased system allows more distant events to be observed. Note that the axis ranges are different between the two panels.

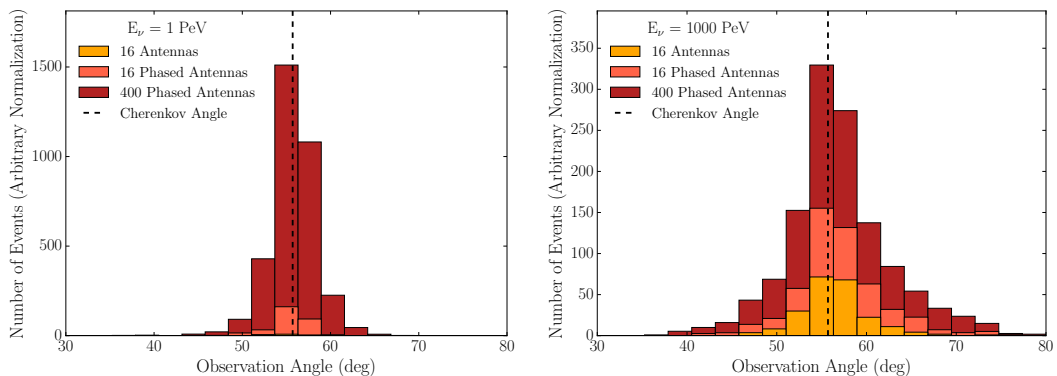


**Figure 9.** The angle of observation of the radio signal compared to the incident neutrino propagation direction for passing events at two different energies (1 PeV and 1000 PeV) and the three different experimental configurations we have discussed (16-channels not phased, a 16-antenna phased array, and a 400-antenna phased array). The Cherenkov angle is shown with a dashed line for reference. Higher energy events are seen farther from the Cherenkov angle, and a phased system allows events to be observed farther from the Cherenkov angle.

The distribution of incident neutrino zenith angles is shown in Figure 10. The events are partitioned into bins of equal solid angle. At 1000 PeV, the acceptance is dominated by events with arrival directions above the horizon due to effective screening by the Earth for

up-going neutrinos. As expected, the zenith angle distribution is broader for 1 PeV neutrinos, for which the interaction length is comparable to the size of the Earth.

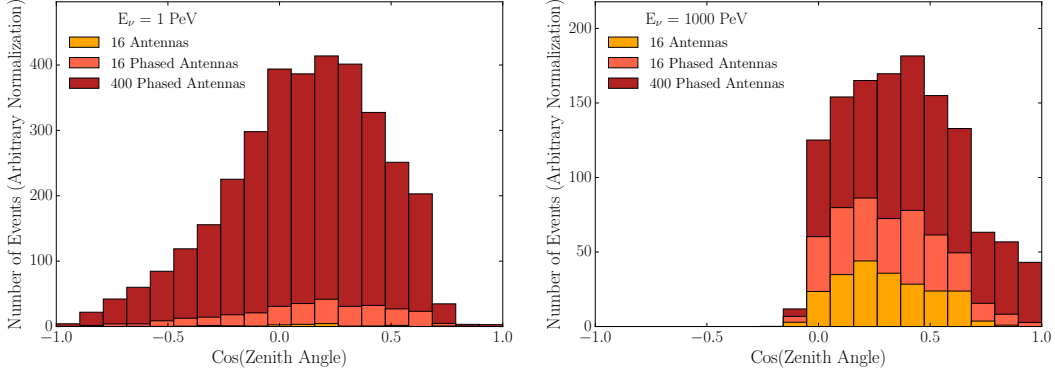


**Figure 10.** The zenith angle of the incident neutrino direction for passing events at two different energies (1 PeV and 1000 PeV) and the three different experimental configurations we have discussed (16-channels not phased, a 16-antenna phased array, and a 400-antenna phased array). The arrays are most sensitive to neutrinos that are slightly down-going.

## References

- [1] IceCube Collaboration, M. G. Aartsen, and et al., *Observation of High-Energy Astrophysical Neutrinos in Three Years of IceCube Data*, *Physical Review Letters* **113** (Sept., 2014) 101101.
- [2] K. Hirata et al., *Observation of a neutrino burst from the supernova sn1987a*, *Phys. Rev. Lett.* **58** (1987) 1490.
- [3] R. M. Bionta et al., *Observation of a neutrino burst in coincidence with supernova 1987a in the large magellanic cloud*, *Phys. Rev. Lett.* **58** (1987) 1494.
- [4] E. Waxman, *IceCube’s Neutrinos: The beginning of extra-Galactic neutrino astrophysics?* (2013), , [arXiv:1312.0558](https://arxiv.org/abs/1312.0558).
- [5] L. A. Anchordoqui, V. Barger, I. Cholis, H. Goldberg, D. Hooper, et al., *Cosmic Neutrino Pevatrons: A Brand New Pathway to Astronomy, Astrophysics, and Particle Physics*, *JHEAp* **1-2** (2014) 1–30.
- [6] K. Murase, *On the origin of high-energy cosmic neutrinos*, in *American Institute of Physics Conference Series*, vol. 1666 of *American Institute of Physics Conference Series*, p. 040006, July, 2015.
- [7] V. S. Beresinsky and G. T. Zatsepin, *Cosmic rays at ultra high energies (neutrino?)*, *Physics Letters B* **28** (Jan., 1969) 423–424.
- [8] K. Greisen, *End to the Cosmic-Ray Spectrum?*, *Physical Review Letters* **16** (Apr., 1966) 748–750.
- [9] G. T. Zatsepin and V. A. Kuz’min, *Upper Limit of the Spectrum of Cosmic Rays*, *Soviet Journal of Experimental and Theoretical Physics Letters* **4** (Aug., 1966) 78.
- [10] The IceCube Collaboration and M. G. e. a. Aartsen, *The IceCube Neutrino Observatory - Contributions to ICRC 2015 Part II: Atmospheric and Astrophysical Diffuse Neutrino Searches of All Flavors*, *ArXiv e-prints* (Oct., 2015) [[arXiv:1510.05223](https://arxiv.org/abs/1510.05223)].

- [11] ANITA Collaboration, P. W. Gorham, and et al., *Observational constraints on the ultrahigh energy cosmic neutrino flux from the second flight of the ANITA experiment*, *Phys. Rev. D* **82** (July, 2010) 022004.
- [12] R. Engel, D. Seckel, and T. Stanev, *Neutrinos from propagation of ultrahigh energy protons*, *Phys. Rev. D* **64** (Nov., 2001) 093010.
- [13] O. E. Kalashev and et al., *Ultrahigh-energy neutrino fluxes and their constraints*, *Phys. Rev. D* **66** (Sept., 2002) 063004.
- [14] M. Ave and et al., *Cosmogenic neutrinos from ultra-high energy nuclei*, *Astroparticle Physics* **23** (Feb., 2005) 19–29.
- [15] V. Barger, P. Huber, and D. Marfatia, *Ultra high energy neutrino nucleon cross section from cosmic ray experiments and neutrino telescopes*, *Physics Letters B* **642** (Nov., 2006) 333–341.
- [16] T. Stanev, *Ultrahigh energy cosmic rays and neutrinos*, *Nuclear Instruments and Methods in Physics Research A* **588** (Apr., 2008) 215–220.
- [17] K. Kotera, D. Allard, and A. V. Olinto, *Cosmogenic neutrinos: parameter space and detectability from PeV to ZeV*, *J. Cosm. and Astropart. Phys.* **10** (Oct., 2010) 13.
- [18] D. Hooper, *Measuring high energy neutrino-nucleon cross sections with future neutrino telescopes*, *Phys. Rev. D* **65** (May, 2002) 097303.
- [19] A. Connolly, R. S. Thorne, and D. Waters, *Calculation of High Energy Neutrino-Nucleon Cross Sections and Uncertainties Using the MSTW Parton Distribution Functions and Implications for Future Experiments*, *Phys.Rev.* **D83** (2011) 113009.
- [20] S. R. Klein and A. Connolly, *Neutrino Absorption in the Earth, Neutrino Cross-Sections, and New Physics (2013)*, , [arXiv:1304.4891](https://arxiv.org/abs/1304.4891).
- [21] P. W. Gorham and et al., *Implications of ultrahigh energy neutrino flux constraints for Lorentz-invariance violating cosmogenic neutrinos*, *Phys. Rev. D* **86** (Nov., 2012) 103006.
- [22] G. Askaryan, *Excess Negative Charge of an Electron-Photon Shower and its Coherent Radio Emission*, *Soviet Physics JETP-USSR* **14 (2)** (1962) 441–443.
- [23] D. Saltzberg and et al., *Observation of the Askaryan Effect: Coherent Microwave Cherenkov Emission from Charge Asymmetry in High-Energy Particle Cascades*, *Physical Review Letters* **86** (Mar., 2001) 2802.
- [24] P. W. Gorham and et al., *Accelerator measurements of the Askaryan effect in rock salt: A roadmap toward teraton underground neutrino detectors*, *Phys. Rev. D* **72** (July, 2005) 023002.
- [25] The ANITA Collaboration, P. W. Gorham, and et al., *Observations of the Askaryan Effect in Ice*, *Physical Review Letters* **99** (Oct., 2007) 171101.
- [26] E. Zas, F. Halzen, and T. Stanev, *Electromagnetic pulses from high-energy showers: Implications for neutrino detection*, *Phys. Rev. D* **45** (Jan., 1992) 362–376.
- [27] J. Avva and et al., *An in situ measurement of the radio-frequency attenuation in ice at Summit Station, Greenland (2014)*, , *J. Glaciol.* **61** (2015) 1005–1011.
- [28] S. Barwick and et al., *South Polar in situ radio-frequency ice attenuation*, *Journal of Glaciology* **51** (2005) 231–238.
- [29] I. Kravchenko and et al., *Updated results from the RICE experiment and future prospects for ultra-high energy neutrino detection at the south pole*, *Phys. Rev. D* **85** (Mar., 2012) 062004.
- [30] ANITA Collaboration, P. W. Gorham, and et al., *The Antarctic Impulsive Transient Antenna ultra-high energy neutrino detector: Design, performance, and sensitivity for the 2006-2007 balloon flight*, *Astroparticle Physics* **32** (Aug., 2009) 10–41.

- [31] P. W. Gorham and et al., *The ExaVolt Antenna: A large-aperture, balloon-embedded antenna for ultra-high energy particle detection*, *Astroparticle Physics* **35** (Dec., 2011) 242–256.
- [32] ARA Collaboration, P. Allison, and et al., *Design and initial performance of the Askaryan Radio Array prototype EeV neutrino detector at the South Pole*, *Astroparticle Physics* **35** (Feb., 2012) 457–477.
- [33] S. W. Barwick and et al., *Design and Performance of the ARIANNA Hexagonal Radio Array Systems (2014)*, , [arXiv:1410.7369](https://arxiv.org/abs/1410.7369).
- [34] ARA Collaboration, P. Allison, and et al., *First Constraints on the Ultra-High Energy Neutrino Flux from a Prototype Station of the Askaryan Radio Array (2014)*, , [arXiv:1404.5285](https://arxiv.org/abs/1404.5285).
- [35] S. W. Barwick and et al., *A first search for cosmogenic neutrinos with the ARIANNA Hexagonal Radio Array*, *Astroparticle Physics* **70** (Oct., 2015) 12–26.
- [36] A. R. Thompson, J. M. Moran, and G. W. Swenson Jr., *Interferometry and Synthesis in Radio Astronomy*. Wiley and Sons, 2 ed., 2001.
- [37] A. Romero-Wolf and et al., *An interferometric analysis method for radio impulses from ultra-high energy particle showers*, *Astroparticle Physics* **60** (2015), no. 0 72 – 85.
- [38] ARA Collaboration and P. e. a. Allison, *Performance of two Askaryan Radio Array stations and first results in the search for ultra-high energy neutrinos*, *ArXiv e-prints* (July, 2015) [[arXiv:1507.08991](https://arxiv.org/abs/1507.08991)].
- [39] S. Buitink and et al., *Searching for neutrino radio flashes from the Moon with LOFAR*, in *American Institute of Physics Conference Series* (R. Lahmann, T. Eberl, K. Graf, C. James, T. Huege, T. Karg, and R. Nahnauer, eds.), vol. 1535 of *American Institute of Physics Conference Series*, pp. 27–31, May, 2013.
- [40] K. Nishimura and et al., *A low-resolution, GSa/s streaming digitizer for a correlation-based trigger system*, , *Proceedings of the Real Time Conference (RT), 18th IEEE-NPSS (2012)*. (2012).
- [41] Koci and Kuivinen, *A 237-meter ice core from South Pole Station*, *Antarctic Journal of the U.S.* **18** (1983), no. 5 113–114.
- [42] P. B. Price and et al., *Temperature profile for glacial ice at the south pole: Implications for life in a nearby subglacial lake*, *Proceedings of the National Academy of Sciences* **99** (2002), no. 12 7844–7847.
- [43] A. J. Gow and et al., *Physical and structural properties of the Greenland Ice Sheet Project 2 ice core: A review*, *Journal of Geophysical Research* **102** (Nov., 1997) 26559.
- [44] J. Alvarez-Muñiz and et al., *Coherent Cherenkov radio pulses from hadronic showers up to EeV energies*, *Astroparticle Physics* **35** (Jan., 2012) 287–299.
- [45] IceCube Collaboration, *Evidence for High-Energy Extraterrestrial Neutrinos at the IceCube Detector*, *Science* **342** (Nov., 2013) 1.
- [46] IceCube Collaboration, M. G. Aartsen, and et al., *Probing the origin of cosmic rays with extremely high energy neutrinos using the IceCube Observatory*, *Phys. Rev. D* **88** (Dec., 2013) 112008.
- [47] A. Aab and et al., *Depth of maximum of air-shower profiles at the Pierre Auger Observatory. II. Composition implications*, *Phys. Rev. D* **90** (Dec., 2014) 122006.
- [48] R. U. Abbasi and et al., *Study of Ultra-High Energy Cosmic Ray composition using Telescope Array’s Middle Drum detector and surface array in hybrid mode*, *Astroparticle Physics* **64** (Apr., 2015) 49–62.
- [49] R. J. Arthern and et al., *Inversion for the density-depth profile of polar firn using a stepped-frequency radar*, *Journal of Geophysical Research: Earth Surface* **118** (2013) 1257.

- [50] P. Allison and et al., *IceRay: An IceCube-centered radio-Cherenkov GZK neutrino detector*, *Nuclear Instruments and Methods in Physics Research A* **604** (June, 2009) 64.
- [51] K.-C. Lai, C.-C. Chen, and P. Chen, *The Strategy of Discrimination between Flavors for Detection of Cosmogenic Neutrinos*, *Nuclear Physics B Proceedings Supplements* **246** (Jan., 2014) 95–98.
- [52] L. Landau and I. Pomeranchuk *Dokl. Akad. Nauk SSSR* **92** (1953) 535.
- [53] A. B. Migdal, *Bremsstrahlung and pair production in condensed media at high energies*, *Phys. Rev.* **103** (1956) 1811.
- [54] I. Kravchenko and et al., *RICE limits on the diffuse ultrahigh energy neutrino flux*, *Phys. Rev. D* **73** (Apr., 2006) 082002.
- [55] J. Alvarez-Muñiz and E. Zas, *The LPM effect for EeV hadronic showers in ice: implications for radio detection of neutrinos*, *Physics Letters B* **434** (Aug., 1998) 396–406.
- [56] J. Alvarez-Muñiz, A. Romero-Wolf, and E. Zas, *Practical and accurate calculations of Askaryan radiation*, *Phys. Rev. D* **84** (Nov., 2011) 103003.
- [57] N. G. Lehtinen and et al., *FORTE satellite constraints on ultrahigh energy cosmic particle fluxes*, *Phys. Rev. D* **69** (Jan., 2004) 013008.
- [58] A. M. Dziewonski and D. L. Anderson, *Preliminary Reference Earth Model (PREM)*, *Phys. Earth Planet. Inter.* **25** (1981) 297.
- [59] S. L. Glashow, *Resonant Scattering of Antineutrinos*, *Physical Review* **118** (Apr., 1960) 316–317.
- [60] V. S. Berezinskiĭ and A. Z. Gazizov, *Cosmic neutrino and the possibility of searching for W bosons with masses 30-100 GeV in underwater experiments*, *Soviet Journal of Experimental and Theoretical Physics Letters* **25** (Mar., 1977) 254.
- [61] V. Berezinsky and A. Gazizov, *Neutrino - electron scattering at energies above the W boson production threshold*, *Sov.J.Nucl.Phys.* **33** (1981) 120–125.
- [62] D. R. Williams, *The Askar’yan effect and detection of extremely high energy neutrinos in the lunar regolith and salt*. PhD thesis, UCLA, 2004.
- [63] C. Balanis, *Antenna Theory: Analysis and Design*. Wiley and Sons, 1 ed., 2005.
- [64] Kraus, *Antennas*. McGraw-Hill, 1 ed., 1950.